

# Size-dependent advection of clouds in exoplanets

**Luis Antonio BALA r0919863,  
Ine MALFAIT r0775938,  
Madhumitha SARAVANAN r0917607.**

Supervisor: Sven KIEFER

# Contents

---

<b>1</b>	<b>Introduction</b>	<b>1</b>
1.1	Cloud particles on exoplanets . . . . .	1
1.2	Chaotic systems . . . . .	1
<b>2</b>	<b>Methods</b>	<b>3</b>
2.1	Simulation . . . . .	3
2.2	Analysis . . . . .	5
2.2.1	Detection of chaos . . . . .	5
2.2.2	Particle radii difference and heterogeneity . . . . .	5
2.2.3	Statistical tests of correlation: the Pearson product-moment measure . . . . .	7
<b>3</b>	<b>Results</b>	<b>8</b>
3.1	Equatorial and pressure slices . . . . .	8
3.2	Lyapunov spectra . . . . .	9
3.3	Pearson correlation coefficient . . . . .	10
<b>4</b>	<b>Discussion</b>	<b>13</b>
4.1	Equatorial and pressure slices . . . . .	13
4.2	Lyapunov spectra . . . . .	14
4.3	Pearson correlation coefficient . . . . .	15
<b>5</b>	<b>Conclusions</b>	<b>17</b>
	<b>Bibliography</b>	<b>17</b>

## Abstract

This report investigates the size dependence of cloud particles advecting in a Hot Jupiter atmosphere and the behaviour of cloud particles (of varying sizes) based on the initial conditions of the cloud particle system using Hot Jupiter GCM simulations. Depending on the sensitivity degree of the initial conditions of the system, the system can be termed as chaotic if the Lyapunov exponent is a positive integer. We calculate the drag force of the gas particle and the equilibrium drift velocity of the cloud particle for a given set of cloud particle radii using hydrodynamic equations. We, then, obtain Lyapunov spectra between the same set of cloud particle radii and find that the system shows a small chaotic behaviour. A correlation between the results can be established using Pearson's correlation method. Understanding the degree of chaos in a cloud particle system being advected in Hot Jupiters can help us model turbulence in climate and atmosphere models of Hot Jupiters more accurately.

---

## Chapter 1

# Introduction

---

### 1.1 Cloud particles on exoplanets

Exoplanetary atmospheres have similar features to that of Earth's atmosphere. The basic photochemistry, transport processes and behaviour of atmospheric constituents (to some extent) are alike. But based on the type of exoplanet, the specifics might vary. This project considers Hot Jupiters - a class of extrasolar gas giants that are physically similar to Jupiters with high surface and atmospheric temperatures and shorter orbital periods ( $P < 10$  days). [1] They are tidally locked (i.e., one side of the planet always facing the star) and are in close proximity to their host stars. So, their dayside surface temperatures are greater than or equivalent to 1000 K. [2] [3] For example, Hot Jupiters are, predominantly, made up of  $H_2$  and He gases.

In Hot Jupiters, the atmospheric particles (gas, dust and cloud) are equally affected by the transport processes like diffusion, advection and convection. In this project, only the advection process is considered. Advection is a process in which a bulk fluid material is displaced from one region to another through its motion. Few models on these Hot Jupiter atmospheres predict high intense winds and super-rotating equatorial jets along with advection. [4] The cloud particles in Hot Jupiters may be chemically rich, i.e., they are not made up of single material but rather they are a mixture of all the materials present. The cloud particles and exoplanet clouds, in general, can be affected by the gas density, temperature and wind speed in the said exoplanet. [5]

When the drag force of the wind is large, the cloud particles move through the atmosphere along with gas particles. On the other hand, when the drag force is not large enough, the cloud particles undergo *gravitational settling*, which is a key process in cloud formation in exoplanets. During gravitational settling, the cloud particles fall through the atmosphere with a terminal or equilibrium drift velocity, which is determined by the particle's size and density. [6] The cloud particle reaches equilibrium drift velocity when the drag force of the fluid acting on it becomes equal to its weight.

### 1.2 Chaotic systems

Chaos theory is a branch of mathematics, and even physics, that investigates the unpredictable behaviour of a non-linear deterministic system. The system is deterministic, i.e. a system in which no randomness is involved in the development of the future state of the system. It will always produce the same output when the initial states don't change. In addition, the system is nevertheless unpredictable, because of the sensitive dependence on the initial conditions. A small error in these initial conditions can produce a completely different output. [7], [8], [9]

A well-known example of chaos is the weather. In 1922, Richardson discovered that weather could be predicted numerically, as a function of wind, temperature, pressure and various other weather variables. Following this discovery, Lorenz, in 1961, developed a simplified model for

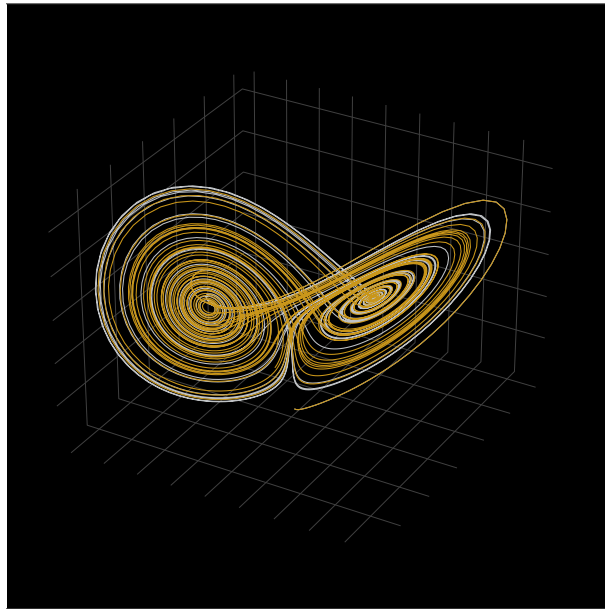


Figure 1.1: Lorenz attractor

the atmospheric convection. This model is now known as the Lorenz attractor, see Figure 1.1. While using the Lorenz attractor, he accidentally discovered that when entering a rounded number used instead of the full number, the result was completely different in the long run. This was the beginning of Chaos Theory, making it clear that weather predictions are impossible to predict in the long term because a small change in the initial conditions can lead to a completely different prediction. [10], [11]

Because it's the Earth's atmosphere, and thus our weather, that behaves chaotically, it is interesting to see if this is also visible in simulations using data from exoplanets. This project investigates the influence of cloud particle size and whether these different sizes cause chaos to occur.

---

## Chapter 2

# Methods

---

### 2.1 Simulation

**General Circulation Model** (GCM or MITgcm) is a model that is devised to study the atmosphere, climate and oceans of a planet. It solves the equations of hydrodynamics, which predict the behaviour of a planet's atmosphere over a period of time. Although GCM was originally designed for Earth's atmosphere and climate, it can also be used to study Hot Jupiter atmospheres. This is done by changing the input parameters (like temperature and pressure conditions) of Earth to that of a Hot Jupiter. Clouds are then incorporated into the results of the temperature profile and winds generated by the GCM. [12]

The simulation code calculates the following quantities, after which it generates three plots: Equatorial slice, Pressure slice and Lyapunov exponent-time graph. (see Subsection 3.1)

- i Calculation of the cloud particle's path: The index of coordinates of the particle at any given time is calculated using the LSODA solver<sup>1</sup>. The values of the velocity of the particle in the x, y and z axes, temperature and density are obtained using linear interpolation in 3D. [13]
- ii Calculation of drag force of the gas particle: Since the behaviour of gas particles around cloud particles changes as the size and drift velocity of the cloud particles changes, it is difficult to calculate the drag force or frictional force for Hot Jupiters. So, the behaviour of gas particles is determined based on two dimensionless numbers, the Knudsen number ( $K_n$ ) and the Reynolds number ( $Re_d$ ).

*Knudsen number* ( $K_n$ ) is the ratio between the mean free path length of the gas particles to the diameter of the cloud particle. [14]

*Reynolds number* ( $Re_d$ ) is the ratio between the inertial force to the drag force and it predicts the fluid flow pattern.

Based on the gas flow in the atmosphere and the interaction of atmospheric particles, we have three cases in which drag force and equilibrium drift velocity can be calculated.

- 1) The free molecular flow ( $K_n \gg 1$ ): The drag force due to elastic collisions between cloud and gas particles is given by [15]

$$\mathbf{F}_{fric}^{sch} = -\pi a^2 \rho |\mathbf{v}| \mathbf{v} \cdot \left[ \left( 1 + \frac{1}{s^2} - \frac{1}{4s^4} \right) erf(s) + \left( \frac{1}{s} + \frac{1}{2s^3} \right) \frac{e^{-s^2}}{\sqrt{\pi}} \right]$$

---

<sup>1</sup>The LSODA solver is a solver for first-order Ordinary Differential Equations (ODEs) that automatically switches between stiff and non-stiff methods based on the data.

where  $s = |\mathbf{v}|/\sqrt{2kT/\bar{\mu}}$ . Here,  $a$  - radius of the cloud particle,  $v$  - drift velocity between cloud particle and gas,  $\rho$  - density of the cloud particle,  $k$  - Boltzmann constant and  $\bar{\mu}$  - mean molecular weight of the gas particle.

- 2) The viscous case ( $K_n \ll 1$ ): The drag force, according to continuum mechanics, is [16]

$$\mathbf{F}_{fric}^{LBS} = -\pi a^2 c_D \frac{\rho}{2} |\mathbf{v}| \mathbf{v}$$

where the drag coefficient,  $c_D$  is given by

$$c_D = \begin{cases} \frac{24}{Re_d} (1 + 0.15 Re_d^{0.687}) & Re_d \leq 500 \\ 9.5 \times 10^{-5} Re_d^{1.397} & 500 < Re_d \leq 1500 \\ 2.61 & Re_d > 1500. \end{cases}$$

Reynolds number is given by  $Re_d = \frac{2a\rho|\mathbf{v}|}{\mu_{kin}}$ , where  $\mu_{kin}$  is the kinematic viscosity of  $H_2$  gas and is defined as  $\mu_{kin} = 5.877 \times 10^{-6} \sqrt{T}$ .

- 3) The general case ( $K_n \approx 1$ ): In this case, the flow is known as *transition flow*. The drag force, here, is found by interpolating drag force terms for high and low Knudsen number limits as shown below, [14]

$$\mathbf{F}_{fric} = \mathbf{F}_{fric}^{sch} \left( \frac{3K_n}{3K_n + 1} \right)^2 + \mathbf{F}_{fric}^{LBS} \left( \frac{1}{3K_n + 1} \right)^2$$

- iii Calculation of equilibrium drift velocity of the cloud particle: The cloud particle falling will accelerate until the drag force and gravitational force acting on it becomes equal, i.e., it attains equilibrium drift velocity. From Newton's law, the expression for equilibrium drift velocity can be written as  $v'_{dr} = |\mathbf{F}_{fric}| + mg$ , where  $m = \frac{4\pi}{3} a^3 \rho$ , is the mass of the cloud particle.
- iv Detection of chaos in the cloud particles' paths: This will be covered in Subsection 2.2.1

In this project, we consider that the clouds are dominated by  $SiO_2$ . Therefore, the parameters in Table 2.1 were chosen. The cloud particles on exoplanets are expected to have a size of around  $1 \times 10^{-6}$  cm. We have done several simulations with particles that have a slightly larger size order, since it doesn't work for this small size. The main simulations are listed in Table 2.2.

Parameter	Value	Units
Mean weight of the cloud particle (m)	$2.35 \times 1.66054 \times 10^{-24}$	g
Density of the cloud particle ( $\rho$ )	2.65	$g \text{ cm}^{-3}$
Maximum time	$10^{6.31}$	s

Table 2.1: Input parameters used in the simulation

Simulation	Radii		
	1	$1 \times 10^{-5}$ cm	$1 \times 10^{-4}$ cm
2	$1 \times 10^{-4}$ cm	$1 \times 10^{-3}$ cm	0.01 cm
3	$1 \times 10^{-3}$ cm	0.01 cm	0.1 cm
4	0.01 cm	0.1 cm	1 cm

Table 2.2: The radii used in the simulations

## 2.2 Analysis

### 2.2.1 Detection of chaos

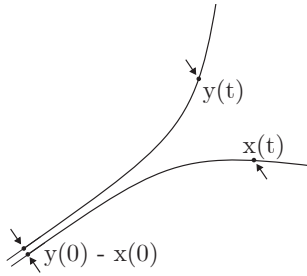


Figure 2.1: The Lyapunov exponent

After running the simulations, these are analysed. This analysis checks whether the particles behave chaotically. Quantitative calculation of chaos is done using Characteristic Lyapunov exponents, which are associated with each trajectory  $\mathbf{x}(t)$ . That indicator calculates the sensitivity degree of the initial conditions of the system. So this means it calculates how unpredictable the system will behave in the long run. Now, any system that has at least one positive Lyapunov exponent is defined as chaotic.[17], [18]

The Characteristic Lyapunov exponent is calculated from the trajectory  $\mathbf{x}(t)$ , for which it holds that  $\mathbf{x}(t+1)$  is calculated from the value of  $\mathbf{x}(t)$ . The stability of this trajectory can be studied by looking at its evolution. Suppose a trajectory  $\mathbf{y}(t)$  arising from the initial condition  $\mathbf{y}(0)$  deviating from  $\mathbf{x}(0)$ :  $\mathbf{y}(t) = \mathbf{x}(0) + \delta\mathbf{x}(0)$ . When the system is not chaotic, the distance between  $\mathbf{x}(t)$  and  $\mathbf{y}(t)$  will remain bounded, or that distance will grow algebraically. But for chaotic systems this is not the case, then that distance grows exponentially with time  $\mathbf{y}(t) - \mathbf{x}(t) \sim [\mathbf{y}(0) - \mathbf{x}(0)]^\gamma$  (see Figure 2.1), where  $\gamma$  is the local exponential acceleration of the divergence. The average exponential acceleration of the divergence is calculated, we can also call it the maximum Lyapunov exponent.[18]

$$\lambda_{max} = \lim_{t \rightarrow \infty} \lim_{\delta(0) \rightarrow 0} \frac{1}{t} \log \left( \frac{\delta(t)}{\delta(0)} \right)$$

It is also interesting to look at the evolution of the Lyapunov exponent. This can be done by plotting a Lyapunov spectrum, where the Lyapunov exponent is plotted against the time step. So at time step  $\tilde{t}$ , we find the Lyapunov exponent  $\lambda(\tilde{t}) = \lim_{\delta(0) \rightarrow 0} \frac{1}{\tilde{t}} \log \left( \frac{\delta(\tilde{t})}{\delta(0)} \right)$

### 2.2.2 Particle radii difference and heterogeneity

The principal aim of the analysis purports to establish the relationship between the radius of the particles and the degree of localised chaos in some predefined system. The trajectories of cloud particles of smaller radii are expected to exhibit more non-linear behaviour by virtue of their lower mass and inertia, as we suspect particles of small-magnitude sizes to be more dynamically sensitive to advection over a given time evolution. It is worth mentioning that the single-molecule composition of the simulation begets the parameters of radius and mass (and thus inertia) as being positively correlated, and we take this as an underlying assumption in

the proceeding analysis.

As the calculated Lyapunov exponent is associated with a given trajectory  $\mathbf{x}(t)$  in the vicinity of the jet stream for a selected time interval in the simulation, it would be conducive to consider a small-number collection of cloud particles as a starting formulation in the characterisation of their behaviour. Since the computation considers the advection of an idealised Hot Jupiter, we only consider a collection of three particles of  $\text{SiO}_2$ , each differing from the other by a singular order of magnitude, as a general proxy for a larger collection of particles. It is helpful to define a new qualitative parameter that will be hereafter referred to as *heterogeneity*, which may be described as the general measure of the difference in magnitude between particle radii for each particle pair in an array of  $n$  particle sizes. A collection of particles of high heterogeneity consists of radii whose differences in magnitude are larger compared to a low-heterogeneity collection. This qualitative degree of heterogeneity, it should be noted, increases with increasing particle radius for our predefined collection, as the arithmetic difference between two particle sizes in an array of three radius elements, increases with comparably larger orders of magnitude.

Another parameter of interest is the quantitative *degree of heterogeneity*. This parameter is computed alongside the qualitative description to function as a correlation pair to compare against the Lyapunov exponent. As the selected particle radii for each collection differ by an order of magnitude, it is appropriate to use a simple geometric mean for each particle pair, then geometrically average the pair once more over the three elements to compute the averaged particle size difference for that collection:

$$\text{degree of heterogeneity} = \sqrt[3]{\sqrt{(r_1 r_2)} \cdot \sqrt{(r_1 r_3)} \cdot \sqrt{(r_2 r_3)}}$$

A final quantitative parameter which will be of analytical use in establishing a numerical relationship between two particle radii (e.g. a particle pair) for a given three-particle collection is the *magnitude of the separation vector* or simply the *separation*, which evaluates the distance between the cloud particles for a given time. We are interested specifically in the time-averaged separation between the particles, which functions as a generalized measure of their relative displacement after some trajectory. Each particle collection yields a total of three particle pairs for three individual separation values, which can be averaged to arrive at an aggregate *mean separation* for the entire particle collection:

$$\bar{d} = \frac{\|\vec{r}_{1,2}\| + \|\vec{r}_{2,3}\| + \|\vec{r}_{1,3}\|}{3}$$

The distances between the particle pairs over the time series (i.e. the magnitudes of the separation vectors) are computed numerically.

Physically, we expect a system of particles of large-magnitude radii (high heterogeneity) to behave more predictably than particles of small-magnitude radii (low heterogeneity), and therefore assume a larger averaged Lyapunov parameter over some chosen time series, although it is entirely possible that individual particle radii could assume a different degree of correlation to the Lyapunov parameter than the measure of heterogeneity. Particles of low heterogeneity (smaller radii difference  $\alpha$  smaller radii) are more likely to have their trajectories displaced by incident advective forces in a turbulent fluid dynamical environment.

### 2.2.3 Statistical tests of correlation: the Pearson product-moment measure

The Lyapunov spectra for each three-element collection of particles alongside their corresponding generated GCM positional plots are likely to provide a descriptive visual overview of the particles' behaviour in the time series and its associated degree of chaos, but a more robust descriptor of such a relationship would involve the application of some statistical test to quantify the extent of their correlation.

As the relationship between particle size dependency and the degree of sensitivity of their trajectories' initial conditions (loosely defined earlier as a general measure of its chaos), the *Pearson product-moment correlation test* is used appropriately in the forthcoming assessment. Similar to other related categories of linear regression, the Pearson correlation test takes two continuous variables and computes the change in magnitude of one input relative to a corresponding change in the magnitude of the other for a given polarity, and arrives at a scaled dimensionless measure of their covariance known as the *Pearson coefficient*  $r$  [19]. For two continuous variables  $x$  and  $y$ , the correlation coefficient  $r$  is given by [20]:

$$r = \frac{\sum_{i=1}^{\infty} (x_i - \bar{x})(y_i - \bar{y})}{\sqrt{[\sum_{i=1}^{\infty} (x_i - \bar{x})^2][\sum_{i=1}^{\infty} (y_i - \bar{y})^2]}}$$

This measure may be used as an interpretative description of the variables' linearity according to the following stratification criteria, for a defined interval of  $-1 \leq r \leq 1$ :

Absolute magnitude of the observed coefficient	Interpretation
0.00 – 0.10	Negligible correlation
0.10 – 0.39	Weak correlation
0.40 – 0.69	Moderate correlation
0.70 – 0.89	Strong correlation
0.90 – 1.00	Very strong correlation

Table 2.3: Sample interpretative stratifications for the Pearson coefficient [19]

A calculated coefficient of positive polarity indicates the two variables to be directly linearly proportional, while a negative polarity signifies an equally inverse proportionality. Pearson coefficients of magnitudes close to 1 express a strong linear association, while magnitudes close to or equal to 0 entail a weak or negligible correlation [21].

The following such assumptions are undertaken as implicit to the Pearson coefficient test as it applies to the analysis [19]: (i) the correlation conforms to an approximately bi-variate normal distribution, and (ii) the covariance between the nominal variables in the scatter demonstrates a degree of interval linearity. Non-monotonic data sets may be utilised in the Pearson framework insofar as the data is normally distributed; other statistical tests may be of use to measure monotonicity instead of linearity, such as Spearman's rank test for correlation, for example. [22].

# Chapter 3

## Results

Chapter 2 explained the methods that would be used to analyse the simulations. In this chapter, the results of the simulations and the analysis will be summed up.

### 3.1 Equatorial and pressure slices

In the first section, the equatorial and pressure slices are presented. Because the trajectories of the particles are independent of the other particles plotted in the same figure, we chose to combine all particle sizes in one equatorial slice (Figure 3.1a) and one pressure slice plot (Figure 3.1b).

In the figure below (Figure 3.1a) the equatorial slices are presented for the particles with radii  $10^{-5}$  cm,  $10^{-4}$  cm,  $10^{-3}$  cm, 0.01 cm, 0.1 cm and 1 cm. It can be noted that the heaviest particles (radii 0.1 cm and 1 cm) descend quickly, while a particle with a radius of 0.01 cm first descends slowly, but after some time descends at the same rate as the heavier particles. The other three particles, the lightest ones, seem to not descend at all. They fluctuate around the height at which they started. It can be seen that the heaviest particle of those three does not fluctuate as much as the two lighter ones, this particle stays mostly at a height of  $1.12 \times 10^{10}$  cm.

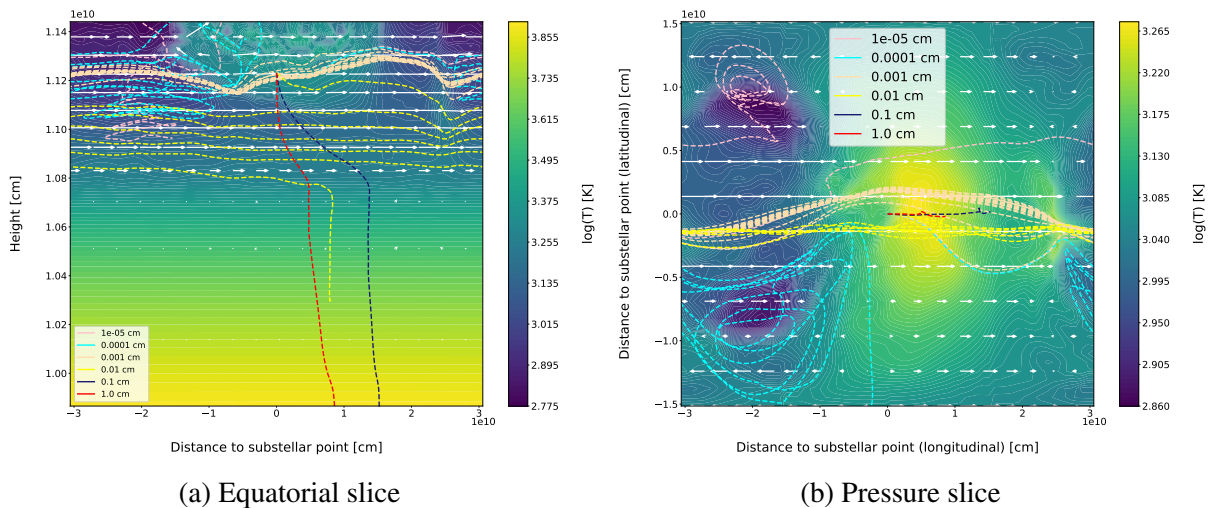


Figure 3.1: The equatorial and pressure slice for particles with radii  $10^{-5}$  cm,  $10^{-4}$  cm,  $10^{-3}$  cm, 0.01 cm, 0.1 cm and 1 cm

In the second figure (Figure 3.1b) the pressure slices are presented for the same particles. In this figure, it is possible to see that the particles not only change the height but also move

relative to the substellar point, where all the particles started their journey. It can be observed that the two heaviest particles (radii 0.1 cm and 1 cm) don't move that much, they only seem to move a bit in the longitudinal direction. The two less heavy particles (radii  $10^{-3}$  cm and 0.01 cm) move a lot in the longitudinal direction but only fluctuate a bit in the latitudinal direction, the two smallest particles (radii  $10^{-5}$  cm and  $10^{-4}$  cm) in the other hand change in both the longitudinal and latitudinal direction. They start taking the same path, but after some time they diverge from each other. The smallest particle, with a radius of  $10^{-5}$  cm, takes a path where it fluctuates around the point at  $1 \times 10^{10}$  cm latitude and  $-2 \times 10^{10}$  cm longitude, while the second-smallest particle, with a radius of  $10^{-4}$  cm, stays in the range of 0 cm to  $-1.5 \times 10^{10}$  cm latitude and 0 cm to  $-3 \times 10^{10}$  cm longitude.

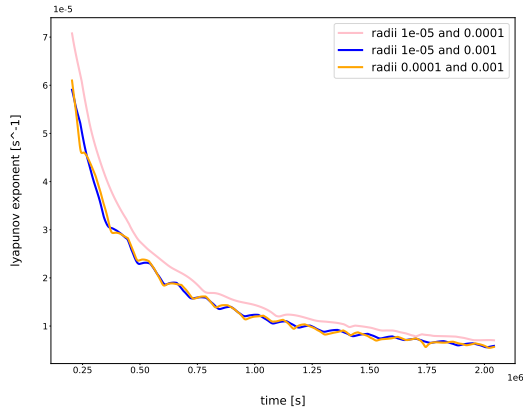
## 3.2 Lyapunov spectra

In the first figure, Figure 3.2a, the Lyapunov spectra for radii  $10^{-5}$  cm and  $10^{-4}$  cm and  $10^{-3}$  cm are shown. The pink Lyapunov exponent calculated for the trajectory of the particles with radii  $10^{-5}$  cm and  $10^{-4}$  cm has the greatest Lyapunov exponent at  $2.04 \times 10^6$  s, with a value of about  $7.04 \times 10^{-6} \frac{1}{s}$ . The orange Lyapunov spectrum, for radii  $10^{-4}$  cm and  $10^{-3}$  cm, has the smallest Lyapunov exponent at the end, with a value of about  $5.66 \times 10^{-6} \frac{1}{s}$ . And the blue Lyapunov spectrum, for radii  $10^{-5}$  cm and  $10^{-3}$  cm, has a value of about  $5.87 \times 10^{-6} \frac{1}{s}$  at the same time. In the figure, it can be seen all spectra have a few valleys. The valleys in the pink spectrum are smaller and less frequent than in the blue and orange spectra.

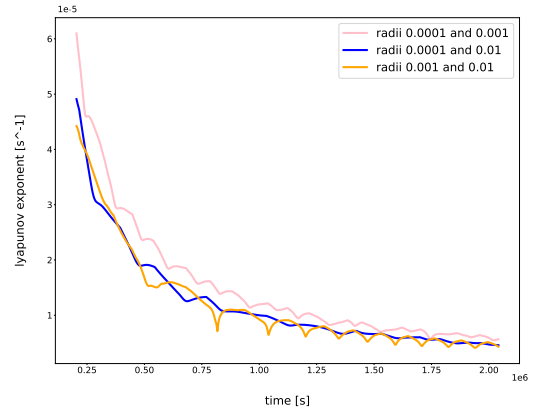
The second figure, Figure 3.2b, presents the Lyapunov spectra for radii  $10^{-4}$  cm and  $10^{-3}$  cm and 0.01 cm. The pink Lyapunov spectrum for radii  $10^{-4}$  cm and  $10^{-3}$  cm is the same one as the orange spectrum in Figure 3.2a. Now, this spectrum has the greatest Lyapunov exponent value of about  $5.66 \times 10^{-6} \frac{1}{s}$  at  $2.04 \times 10^6$  s. The blue Lyapunov spectrum for radii  $10^{-4}$  cm and 0.01 cm is the second greatest with a value of about  $4.58 \times 10^{-6} \frac{1}{s}$  at  $2.04 \times 10^6$  s. The last, orange, Lyapunov spectrum for radii  $10^{-3}$  cm and 0.01 cm has a value of about  $4.31 \times 10^{-6} \frac{1}{s}$  at  $2.04 \times 10^6$  s but jumps a few times over the blue spectrum. Just like in Figure 3.2b, it can be noted that all spectra have a few valleys.

In Figure 3.2c the Lyapunov spectra for radii  $10^{-3}$  cm, 0.01 cm and 0.1 cm can be observed. Just as before, the pink spectrum for radii  $10^{-3}$  cm and 0.01 cm is the same as the orange in Figure 3.2b, and thus has a value of about  $4.31 \times 10^{-6} \frac{1}{s}$ . This is the only spectrum that goes on to the end of the simulation after  $2.04 \times 10^6$  s, the two other Lyapunov spectra end at  $6.95 \times 10^5$  s. At this moment, the orange spectrum for radii 0.01 cm and 0.1 cm is the biggest with a Lyapunov exponent value of  $10.81 \times 10^{-6} \frac{1}{s}$ . The blue spectrum for radii  $10^{-3}$  cm and 0.1 cm has a Lyapunov exponent value of  $9.63 \times 10^{-6} \frac{1}{s}$ . Again, it can be seen that the spectra have valleys.

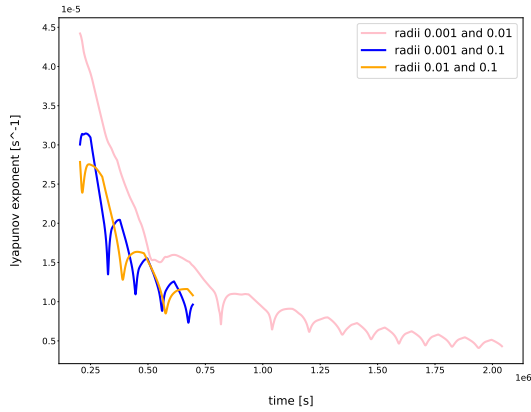
In the last figure, Figure 3.2d, the Lyapunov spectra for radii 0.01 cm, 0.1 cm and 1 cm are shown. Again, the pink spectrum for radii 0.01 cm and 0.1 cm is the same as the orange Lyapunov spectrum in Figure 3.2c, which means it has a Lyapunov exponent value of  $10.81 \times 10^{-6} \frac{1}{s}$  at  $6.95 \times 10^5$  s. It can be noted that the blue Lyapunov spectrum for radii 0.01 cm and 1 cm has a value of  $4.75 \times 10^{-6} \frac{1}{s}$  at  $7.38 \times 10^5$  s. The orange spectrum, for radii 0.1 cm and 1 cm, has a value of  $6.26 \times 10^{-6} \frac{1}{s}$  at  $6.95 \times 10^5$  s. The only Lyapunov spectrum that



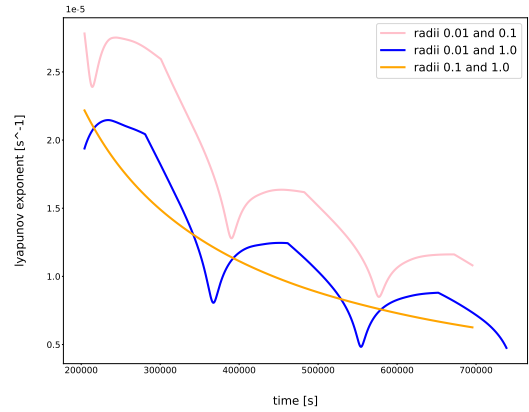
(a) The Lyapunov spectrum of cloud particles of radii  $10^{-5}$  cm,  $10^{-4}$  cm and  $10^{-3}$  cm



(b) The Lyapunov spectrum of cloud particles of radii  $10^{-4}$  cm,  $10^{-3}$  cm and  $0.01$  cm



(c) The Lyapunov spectrum of cloud particles of radii  $10^{-3}$  cm,  $0.01$  cm and  $0.1$  cm



(d) The Lyapunov spectrum of cloud particles of radii  $0.01$  cm,  $0.1$  cm and  $1$  cm

Figure 3.2: The Lyapunov spectra

does not have valleys, in this figure, is the orange one for radii  $0.1$  cm and  $1$  cm. The other two spectra have a few valleys.

### 3.3 Pearson correlation coefficient

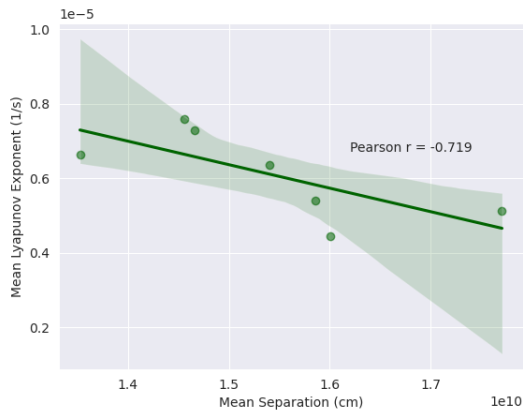
The main parameters of interest to the analysis (the mean separation and Lyapunov values) – together with the aggregated Pearson coefficient for the entirety of the seven, three-particle collection data sets – are summarised in Table 3.1. The aggregated tabulated data summarises the heterogeneity degree and the particle collections (of gradually increasing orders of magnitude) according to appropriate qualitative classification strata, with each heterogeneity criterion assuming a corresponding mean separation and mean Lyapunov value:

Heterogeneity	3-Particle System $[r_1, r_2, r_3]$ (cm)	Mean Separation (cm)	Mean Lyapunov (1/s)
Very low	$[1 \times 10^{-5}, 1 \times 10^{-4}, 1 \times 10^{-3}]$	$1.5402 \times 10^{10}$	$6.3666 \times 10^{-6}$
Low	$[5 \times 10^{-5}, 5 \times 10^{-4}, 5 \times 10^{-3}]$	$1.5858 \times 10^{10}$	$5.3954 \times 10^{-6}$
Medium-low	$[1 \times 10^{-4}, 1 \times 10^{-3}, 1 \times 10^{-2}]$	$1.7709 \times 10^{10}$	$5.1213 \times 10^{-6}$
Medium	$[3 \times 10^{-4}, 3 \times 10^{-3}, 3 \times 10^{-2}]$	$1.6004 \times 10^{10}$	$4.4378 \times 10^{-6}$
Medium-high	$[1 \times 10^{-3}, 1 \times 10^{-2}, 1 \times 10^{-1}]$	$1.4454 \times 10^{10}$	$7.5888 \times 10^{-6}$
High	$[3 \times 10^{-3}, 3 \times 10^{-2}, 3 \times 10^{-1}]$	$1.3524 \times 10^{10}$	$6.6417 \times 10^{-6}$
Very high	$[1 \times 10^{-2}, 1 \times 10^{-1}, 3 \times 10^0]$	$1.4665 \times 10^{10}$	$7.2979 \times 10^{-6}$

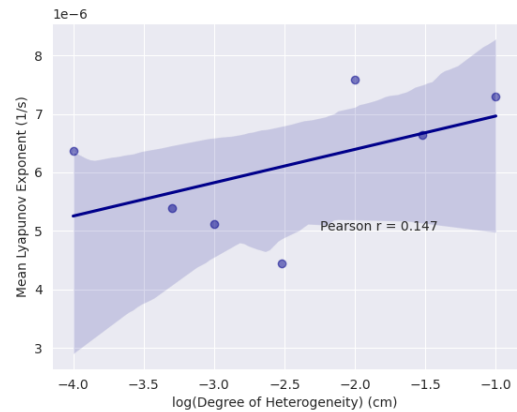
Table 3.1: Mean separation and Lyapunov exponent values for seven three-particle systems of varying radii heterogeneity

The intermediate averaged separation values and Lyapunov exponents (for the low, medium, and high cases) falling in between the principal four data sets are included in the tabulation to satisfy an appropriate sample size for the Pearson test. A numerical coefficient of 5 was selected for the radii of the intermediate low-heterogeneity case as the simulation is unable to run for adjacent integer values apart from 0, 1, or 5 for that particular small-radius regime, while a coefficient of 3 was selected for the medium- and high-heterogeneity cases as those values fall closer to an intermediate numerical point between the heterogeneity strata above and below those cases.

A scatter diagram with a corresponding best-fit was generated for the following two correlation pairs from the data sets in Table 3.1: (mean separation, mean Lyapunov) and (heterogeneity degree, mean Lyapunov):



(a) Scatter plot and regression line of mean Lyapunov exponent vs. mean separation



(b) Scatter plot and regression line of mean Lyapunov exponent vs. heterogeneity degree

Figure 3.3: Scatter plots of correlation variables

The translucent bands around the trend lines indicate the confidence interval of the scatter (CI = 0.95). A wideband confidence interval is expected for scatters involving smaller data sets, and is accentuated for variables of weak correlation strength, as is the case in Figure

3.3b. The data points corresponding to the degree of heterogeneity are linearised by assuming the logarithm of the argument to produce a correlation with appropriate linear intervals.

Figure 3.3b is a direct graphical visualisation of the mean Lyapunov and heterogeneity columns from Table 3.1, while Figure 3.3a takes the mean separation column and ranks the elements by magnitude, decoupling the data set from the original heterogeneity order. This allows the linear association of the Lyapunov-separation pair to be more clearly distinguished from the Lyapunov-heterogeneity pair.

The Pearson correlation coefficient was calculated for the entire data set for Table 3.1, with the mean separation and the mean Lyapunov exponent assuming the continuous variables  $x_i$  and  $y_i$  from the Pearson correlation equation, respectively. The correlation pairs selected for the correlation analysis are the heterogeneity (degree of radii difference of a particle) *and* the mean particle separation to the mean Lyapunov exponent.

Pair of correlation variables	Pearson coefficient
Heterogeneity (radii difference) and mean Lyapunov exponent	0.147
Mean particle separation and mean Lyapunov exponent	-0.719

Table 3.2: Pearson correlation coefficients for the variables of interest

The computed Pearson coefficients from the Pearson product-moment equation are 0.147 for the degree of the particle size difference and the mean Lyapunov exponent, and  $-0.719$  for the mean particle separation and the mean Lyapunov exponent, both indicating weak and strong correlations respectively, but of opposing directionality.

---

## Chapter 4

# Discussion

---

In this chapter, we will analyse the results given in Chapter 3. Firstly the equatorial and pressure slices are analysed, after that the results in the Lyapunov spectra will be discussed. At last, the Pearson correlation coefficients that were found are explained.

### 4.1 Equatorial and pressure slices

In this section, we try to find out if two particles with similar sizes would behave chaotically. We do this by combining the information received from both the equatorial slice (Figure 3.1a) and the pressure slice (Figure 3.1b) and our knowledge about chaos. In Chapter 1.2 it was explained that a chaotic system has sensitive dependence on the initial conditions. In Section 4.2 we will compare the Lyapunov exponents we found and showed in Section 3.2 and the expectations we write down here.

We start by looking at the two lightest particles, those with radii of  $10^{-5}$  cm and  $10^{-4}$  cm. In the first few steps they follow the same trajectory, but at some point, the lightest particle starts to fluctuate around the point at  $1 \times 10^{10}$  cm latitude and  $-2 \times 10^{10}$  cm longitude. The behaviour we see for this cloud particle reminds us of the Lorentz attractor. Because the two particles did diverge rather quickly in the latitudinal and longitudinal direction, as we can see in the pressure slice (Figure 3.1b), we would suspect that the Lyapunov exponent would be greater than zero, so we would be able to say that there is chaos here.

Now we take a look at the lightest particle, with a radius of  $10^{-5}$  cm, and the particle with a radius of  $10^{-3}$  cm. Again, the first few steps look the same for these particles, but the lightest particle changes its height at some point while the particle with a radius of  $10^{-3}$  cm stays at almost the same height at all times. Because the two particles did diverge rather quickly, in the latitudinal and longitudinal direction as well as in the height, we again can suspect that we have a chaotic system. The particle with a radius of  $10^{-3}$  cm circles around the planet, which leads to a fluctuating distance in the longitudinal direction. Because the distance between the two particles in the latitudinal is not as big as for the two lightest particles, we expect to find a smaller Lyapunov exponent, which is still bigger than zero.

It is also interesting to study the particle behaviour of the particle with a radius of  $10^{-4}$  and the particle with a radius of  $10^{-3}$ . These particles start on the same path, but diverge when the lightest particle changes its height. Just like the two times before, we would expect to find that this could be a chaotic system, but with a Lyapunov exponent smaller than the first one, because the latitudinal distance does not get as big.

Now, look at the particles with radii of  $10^{-4}$  cm and 0.01 cm. We see in Figure 3.1a, that the particles diverge almost directly, the heaviest particle loses height, while the lightest particles go up higher in the atmosphere. We see that this behaviour continues throughout the whole simulation. In Figure 3.1b, we see that the particles diverge a bit in the latitudinal direction.

We expect to find a Lyapunov exponent similar to the one we found for radii  $10^{-4}$  cm and  $10^{-3}$  cm.

The particles with radii  $10^{-3}$  cm and 0.01 cm have a similar trajectory when looking at Figure 3.1b. They mostly differ in their height, but also latitudinal and longitudinal direction. This leads to a Lyapunov exponent a bit smaller than the one before, for radii  $10^{-4}$  cm and 0.01 cm.

Now we take a look at the particles with radii of  $10^{-3}$  cm and 0.1 cm. Again, these particle trajectories seem to mostly differ in their height, but now they also differ in their longitudinal direction. The lightest particle moves around the planet, while the heavier particle drops. Their latitudinal distance doesn't make a big difference in the total distance between the two particles. This leads to a small Lyapunov exponent, still bigger than zero. The particles with radii 0.01 cm and 0.1 cm and the particles with radii 0.01 cm and 1 cm seem, just like before, mostly to differ in their height. So we expect Lyapunov exponents similar to the Lyapunov exponent found for radii  $10^{-3}$  cm and 0.1 cm.

We see that the two heaviest particles with radii of 1 cm and 0.1 cm behave similarly, so this looks like they don't behave completely chaotically. They have the same latitudinal distances, and after they moved away from each other for a short distance, they lose height at a path that looks almost parallel to the path of the other particle. So this suggests that the Lyapunov exponent would be rather close to zero. But because the heaviest particle falls faster than the other particle, the distance has a height and a longitudinal aspect.

## 4.2 Lyapunov spectra

Firstly, looking at the results, we can see that all Lyapunov exponents found are small ( $\sim 10^{-6} \frac{1}{s}$ ). This means that although all Lyapunov exponents are greater than zero, there isn't much chaos in this system. Whereas all Lyapunov exponents are greater than zero, this system is defined as chaotic (see Section 2.2.1).

Secondly, we look at all the figures, where we find some recurring developments.

- We notice that the Lyapunov exponent is generally the biggest for the smallest particles. This means that for the real particle size, we probably would have an even bigger Lyapunov exponent.
- The next thing that stands out is the valleys we see in the Lyapunov spectra, these can be explained: we get those dips only when the particles move all over the planet, so when we see bands in both the equatorial and pressure slices for the longitudinal direction. The distance between the two particles will then become larger and smaller as the particles get farther and closer.
- The last thing that should be explained is why the Lyapunov exponents sometimes are shorter than the others. This is because one of the particles or both particles reaches the ground (height = 0 cm). When this happens, the rest of the simulation isn't useful any more, so we don't take that part into account for the results.

In general, our results seem to fit with the things we expected for the equatorial and pressure slice (see Figures 3.1a and 3.1b) and reported in Section 4.1.

### 4.3 Pearson correlation coefficient

The numerical trend cohering the heterogeneity or the general measure of particle radii difference with the separation and Lyapunov parameters in Table 3.1 is not evident upon initial scrutiny and appears to form a semi-random scatter if the data sets are selected to be ordered or ranked according to the increasing magnitude of the radii heterogeneities. A different rank (i.e. by increasing mean separation instead of increasing heterogeneity) sheds to light a higher-strength correlation pattern between the averaged separation and Lyapunov values.

An important remark ought to be made at the onset of the analysis: while the Lyapunov exponents from the previous section assume certain trends with the radius for *localised* particle-pair behaviour, the overall correlation behaves differently when considering the entire collection of three particles. This slight eccentricity in behaviour could be the result of numerical averaging of the Lyapunov parameters over the entire collection, which renders the distinction of the correlation for each particle-pair to be slightly difficult to parse from the aggregated Lyapunov exponent.

A preliminary overview of the heterogeneity-Lyapunov correlation from the values in Table 3.1 appears to signify a weakly correlated relationship for this particular rank, although it is notable that the Lyapunov exponent steadily decreases by approximate increments of  $0.5000 \times 10^{-6}$  up until the medium-heterogeneity case, from which the parameter shoots up to a local extremum in the medium-high case and settles at a relatively high regime for the largest particle radii, as is evidently seen by the deviated scatter in Figure 3.3b.

A possible reason for this trend may lie in low-heterogeneity particles of smaller radii and lower inertia being more susceptible to trajectory displacements from the dynamical forces in the jet stream, which was observed from the previous Lyapunov spectra graphs. The particle trajectories are potentially expected to behave less non-linearly as their inertial mass for increasing particle radii and heterogeneity increase up until a certain threshold, whereupon gravitational settling [5] or the largest particle sizes in the high-heterogeneity collection emerges as the dominant dynamical effect and assumes responsibility for the local Lyapunov extremum. As the trend between the variables experiences a change in directional behaviour in the data set by virtue of the advection-particle interaction present in the physical system, the Pearson test registers the degree of chaos and the particle radii difference as a weak correlation.

Similarly, if we are to consider the heterogeneity-separation correlation, the trend points to a negligible association with no apparent association for increasing values of the heterogeneity and demonstrates an even greater random scatter in the values compared to the previous correlation pair, although it should be noted that this variable pair is of passing interest to the analysis, as we are largely concerned with the association of the variables to the Lyapunov exponent itself.

The mean separation-Lyapunov correlation, on the other hand, upon ranking the values from smallest to largest mean separation (regardless of the analogous heterogeneity), appears to express the *greatest* correlation strength among the reported correlation pairs, which may be corroborated by the magnitude of their Pearson coefficient in Table 3.2. The comparatively

closely-bound data points relative to the line of regression in Figure 3.3a graphically indicates a higher-strength linear scatter. The mean separation appears to be a more reliable predictor of the non-linearity of the particles' trajectories compared to the variable of the particle size difference (heterogeneity).

The pressure slice positional maps serve as a visual indication of the underlying dynamics behind the correlation: we expect the mean separation of a system of particles to be at its local maximum for smaller particle radii to be significantly *higher* due to their susceptibility to being advected into more turbulent trajectories. The characteristic swirling pattern formed by these path vortices is a distinct qualitative expression of dynamical non-linearity, which agrees with the computed Lyapunov exponents as it correlates to their divergent behaviour. For small particles in a hydrodynamically active environment, turbulent velocity gradients tend to indeed induce more chaotic orientations [23].

Regarding the significance of the values upon examining the parameters individually, the positive Lyapunov exponent values entail a minimal amount of chaos in the advective system as  $\lambda(t) > 0$ , although the degree of non-linearity for each of the particle collections is minimal with numerical variations in the order of  $10^{-6}$ . Thus, it would be remiss to characterise the trajectories as *significantly* disordered, despite their satisfying the Lyapunov criteria for chaos.

The data purports no direct relationship among heterogeneity, separation, and the numerical degree of chaos, as the correlation pairs among the three variables of interest assume different signatures of linearity, and it would thus be of no analytic use to speak of a direct three-variable correlation. The three parameters taken together assume no shared statistical directionality.

Heterogeneity and the mean Lyapunov exponent share a positive correlation of weak strength, while the mean particle separation and the mean Lyapunov exponent share a negative correlation of moderately high strength, as defined by our earlier stratification criteria. The opposing Pearson strengths for the two correlation pairs owe themselves to the complex interplay between kinematic environmental variables (e.g. advection, gravity) and the numerical sensitivity of their trajectories during initial conditions, as was discussed earlier.

---

## Chapter 5

# Conclusions

---

In this report, we have investigated the size dependence of cloud particles ( $SiO_2$ ) when advected in the atmosphere of Hot Jupiters and how different cloud particle sizes behave over a period of time, i.e., if the behaviour is chaotic or not. The Hot Jupiter GCM simulation, using necessary equations to calculate the drag forces acting on the cloud particle and its equilibrium drift velocity, generates three plots: Equatorial slice, Pressure slice and Lyapunov spectrum.

- i From the equatorial slice, it is evident that the heavier cloud particles (of sizes 1 cm and 0.1 cm) descend quickly while the lighter particles (of sizes  $10^{-3}$  cm,  $10^{-4}$  cm,  $10^{-5}$  cm) does not appear to descend. Meanwhile, the descent of a cloud particle of intermediate size (0.01 cm) seems very slow until it reaches the height of around  $1.08 \times 10^{10}$  cm, after which it rapidly falls as heavier particles did.
- ii In the pressure slice, the particles move with respect to both height and substellar point (initial position of the particles). Cloud particles of size 0.1 cm and 1 cm seem to move longitudinally. While the other lighter particles (of sizes 0.01 cm,  $10^{-3}$  cm,  $10^{-4}$  cm and  $10^{-5}$  cm) move in both latitudinal and longitudinal direction. In particular, the lighter particles (of size  $10^{-4}$  cm,  $10^{-5}$  cm) diverge from each other after some time.
- iii In the obtained Lyapunov spectra between particles of different sizes, the Lyapunov exponents are found to be small positive integers (in the order of  $10^{-6} \frac{1}{5}$ ). This shows that there is not much chaos in the system, even though, the Lyapunov exponents are greater than zero. As expected, an inverse relationship between the Lyapunov exponents and the size of the cloud particle can be observed in the Lyapunov spectra. Although, this trend does not hold for some particle pairs. This could be due to various factors at hand like advection, gravity and the sensitivity degree of the initial conditions of the cloud particle system.

Lastly, the Pearson correlation coefficient was found to establish a correlation between the results obtained. The heterogeneity and the mean Lyapunov exponent have a positive correlation of weak strength (Pearson coefficient,  $r = 0.147$ ) whereas the mean cloud particle separation and the mean Lyapunov exponent have a negative correlation of moderately high strength (Pearson coefficient,  $r = -0.719$ ). By understanding the degree of chaos in a cloud particle system being advected in a Hot Jupiter, especially noting how lighter particles lean towards more chaotic behaviour than their heavier counterparts, climate and atmospheric conditions of Hot Jupiters can be appropriately modelled. There are few future prospects for this project:

- The GCM simulations were run with the cloud particles located at the starting of the grid. The results might be different when we vary the starting position of the particle within the simulation.
- This project can be expanded to include other transport processes like diffusion and convection and observe how chaotic its behaviour can get. Including all the transport processes might give us a better understanding into the climate of Hot Jupiters.

# Bibliography

---

- [1] Ji Wang, Debra A. Fischer, Elliott P. Horch, and Xu Huang. On the occurrence rate of hot jupiters in different stellar environments. *The Astrophysical Journal*, 799(2):229, jan 2015.
- [2] John Wenz. Lessons from scorching hot weirdo-planets. <https://knowablemagazine.org/article/physical-world/2019/hot-jupiter-formation-theories>.
- [3] Rosalba Perna, Kristen Menou, and Emily Rauscher. Magnetic drag on hot jupiter atmospheric winds. *The Astrophysical Journal*, 719(2):1421, jul 2010.
- [4] Emily Rauscher and Kristen Menou. Three-dimensional modeling of hot jupiter atmospheric flows. *The Astrophysical Journal*, 714(2):1334, apr 2010.
- [5] Christiane Helling. Exoplanet clouds. *Annual Review of Earth and Planetary Sciences*, 47(1):583–606, 2019.
- [6] Peter Woitke and Ch. Helling. Dust in brown dwarfs. ii. the coupled problem of dust formation and sedimentation. *Astronomy and Astrophysics*, 399:297–313, 2003.
- [7] Encyclopaedia Britannica. Chaos theory. <https://academic-eb-com.kuleuven.e-bronnen.be/levels/collegiate/article/chaos-theory/22470>.
- [8] Wikipedia. Chaos theory. [https://en.wikipedia.org/wiki/Chaos\\_theory](https://en.wikipedia.org/wiki/Chaos_theory).
- [9] Wikipedia. Deterministic systems. [https://en.wikipedia.org/wiki/Deterministic\\_system](https://en.wikipedia.org/wiki/Deterministic_system).
- [10] Roberto Buizza. *Chaos and Weather Prediction*. ECMWF, 2002.
- [11] Wikipedia. Edward norton lorenz. [https://en.wikipedia.org/wiki/Edward\\_Norton\\_Lorenz](https://en.wikipedia.org/wiki/Edward_Norton_Lorenz).
- [12] Michael T. Roman, Eliza M.-R. Kempton, Emily Rauscher, Caleb K. Harada, Jacob L. Bean, and Kevin B. Stevenson. Clouds in three-dimensional models of hot jupiters over a wide range of temperatures. i. thermal structures and broadband phase-curve predictions. *The Astrophysical Journal*, 908(1):101, feb 2021.
- [13] rdrv.io. lsoda: Solver for ordinary differential equations (ode). <https://rdrr.io/cran/deSolve/man/lsoda.html>.
- [14] Woitke, P. and Helling, Ch. Dust in brown dwarfs - ii. the coupled problem of dust formation and sedimentation. *A&A*, 399(1):297–313, 2003.

- [15] George J Maslach and Samuel Albert Schaaf. Cylinder drag in the transition from continuum to free-molecule flow. *The Physics of Fluids*, 6(3):315–321, 1963.
- [16] S Lain, D Bröder, and M Sommerfeld. Experimental and numerical studies of the hydrodynamics in a bubble column. *Chemical Engineering Science*, 54(21):4913–4920, 1999.
- [17] Alan Wolf, Jack B. Swift, Harry L. Swinney, and John A. Vastano. Determining lyapunov exponents from a time series. *Physica. D*, 16(3):285–317, 1985.
- [18] Angelo Vulpiani, Fabio Cecconi, and Massimo Cencini. *Chaos: from simple models to complex systems*, volume 17. World Scientific, 2009.
- [19] Patrick Schober, Christa Boer, and Lothar Schwarte. Correlation coefficients: Appropriate use and interpretation. *Anesthesia and Analgesia*, 126:1, 02 2018.
- [20] Mavuto Mukaka. Statistics corner: A guide to appropriate use of correlation coefficient in medical research. *Malawi medical journal : the journal of Medical Association of Malawi*, 24:69–71, 09 2012.
- [21] Wilhelm Kirch, editor. *Pearson's Correlation Coefficient*, pages 1090–1091. Springer Netherlands, Dordrecht, 2008.
- [22] Andrijana Eđed Rebekić, Zdenko Lončarić, Sonja Petrovic, and Sonja Marić. Pearson's or spearman's correlation coefficient - which one to use? *Poljoprivreda*, 21:47–54, 12 2015.
- [23] Y. Wang, J. Kao, S. Weinbaum, and R. Pfeffer. On the inertial impaction of small particles at the entrance of a pore including hydrodynamic and molecular wall interaction effects. *Chemical Engineering Science*, 41(11):2845–2864, 1986.